Laser direct writing pattern structures on AgInSbTe phase change thin film

Aihuan Dun (顿爱欢)[1,2], Jingsong Wei (魏劲松)[1*], and Fuxi Gan (干福熹)[1]

[1]*Shanghai Institute of Optics and Fine Mechanics, Chinese Academy of Sciences, Shanghai 201800, China*

[2]*Graduate University of Chinese Academy of Sciences, Beijing 100049, China*

[*]*Corresponding author: weijingsong@siom.ac.cn*

Received December 31, 2010; accepted March 15, 2011; posted online May 31, 2011

Different pattern structures are obtained on the AgInSbTe (AIST) phase change film as induced by laser beam. Atomic force microscopy (AFM) was used to observe and analyze the different pattern structures. The AFM photos clearly show the gradually changing process of pattern structures induced by different threshold effects, such as crystallization threshold, microbump threshold, melting threshold, and ablation threshold. The analysis indicates that the AIST material is very effective in the fabrication of pattern structures and can offer relevant guidance for application of the material in the future.

OCIS codes: 210.4810, 180.6900.

doi: 10.3788/COL201109.082101.

Micro- or nano-structuring of surfaces of various thin film materials with thickness ranging from several nanometers to micrometers is the main development trend in recent pattern structure applications[1−3]. One of the most interesting and viable methods for the fabrication of high aspect-ratio pattern structures is the laser direct writing technology. The advantages of the technology include a processing area, with a measurement within a micrometer to a sub-micrometer range and non-contact and nonplanar processing characteristic, which is not commonly found in other technologies[1,4].

Chalcogenide phase change materials have been extensively investigated and used as optical and nonvolatile electrical data storage media due to the apparent difference in optical reflectivity and electrical resistivity between the crystalline and amorphous states[5−13]. One of the most commonly used chalcogenide materials is $Ag_8In_{14}Sb_{55}Te_{23}$(AIST). Under laser irradiation, AIST is capable of achieving different threshold effects based on the increase of the laser energy to certain values. The effects correspond to different morphologies. Based on the property of the material, different pattern structures can be obtained by adjusting precisely the laser energy. Compared with photoresist, which is generally used for the fabrication of pattern structures, AIST phase change material presents more advantages. Firstly, the material is sensitive to irradiation intensity of laser beam with different wavelengths. Secondly, different pattern structures can be obtained by controlling precisely the laser beam energy. Most importantly, this material does not need developing or etching process, thereby reducing time consumption and cost. In this letter, we obtain different pattern structures on AIST phase change film by laser direct writing technology and use atomic force microscopy (AFM) to observe and analyze the pattern structure morphology. The gradually changing process of the pattern structures on AIST material is addressed as well. The experimental results and analysis indicate that AIST material is effective in the fabrication of different pattern structures.

Single-layered amorphous AIST thin film was directly deposited on K9 glass substrate by radio frequency magnetron-control sputtering method at room temperature. The background pressure was approximately 1.5×10^{-4} Pa and the sputtering pressure was approximately 0.8 Pa of the Ar environment. Sputtering power was 70 W and the thin film thickness was approximately 200 nm. The laser direct writing system used a red laser beam (λ = 635 nm) and the laser beam was focused through an objective lens and irradiated on the AIST film. The laser power ranged from 1 to 8 mW. Different pattern structures corresponding to different threshold effects were observed using atomic force microscope (AFM, Veeco, Multimode V). After irradiation by pulse laser, the sample was further subjected to a chemical etching process in NaOH solution with 1.0 wt.-% concentration for 3 min to examine the difference between the amorphous state and crystalline state. Subsequent to the etching process, the change of the surface sample was re-examined by the same AFM.

Figure 1 presents the results of laser-induced crystallization on AIST film by red laser with laser power of 1.2 mW. Figure 1(a) is the crystallized spot induced by pulse laser with a width of 50 ns and size of approximately 1 μm. Figure 1(c) is the crystallized line with a size of approximately 3 μm and which was induced by continuous-wave (CW) laser beam. The obvious color difference between the as-deposited film and the crystallized area can be observed. The contour lines of the two kinds of crystallized areas in Figs. 1(b) and (d) show that the depth of this area is approximately 10 nm, which is approximately 5% of the thickness of the film. This volume shrinkage effect is mainly due to the density difference between the amorphous and crystalline states[14,15]. During laser irradiation, AIST film is transformed into a face-centered-cubic (fcc-type) structure from amorphous state at approximate 440 K, and continued to transform into a hexagonal-close-packed (hcp-type) structure at approximate 620 K[10,16,17]. The density of the crystallized state is 5% larger than the amorphous state; thus, the volume of the material is bound to decrease after the transformation.

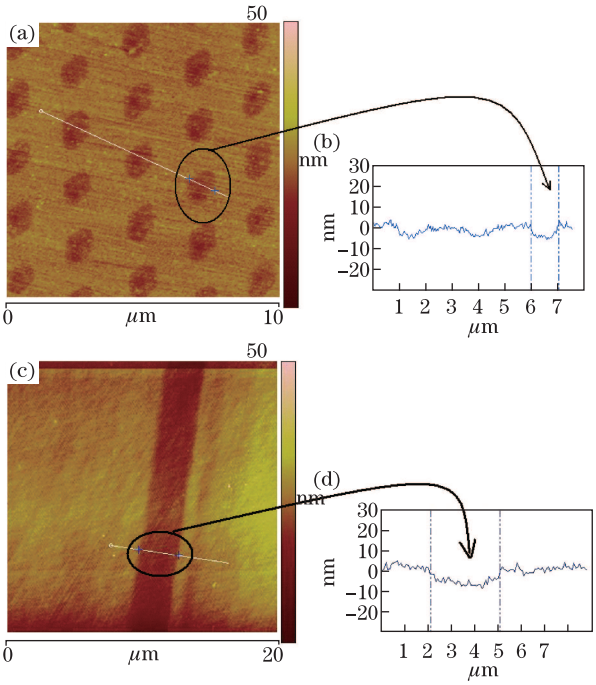

Fig. 1. Laser-induced crystallization on AIST film by red laser. (a) AFM two-dimensional (2D) photos of the crystallized spot induced by pulse laser ($\lambda = 635$ nm); (b) contour lines of the crystallized spot marked by circle in (a); (c) AFM 2D photos of the crystallized line induced by CW laser ($\lambda = 635$ nm); (d) contour lines of the crystallized line marked by circle in (c).

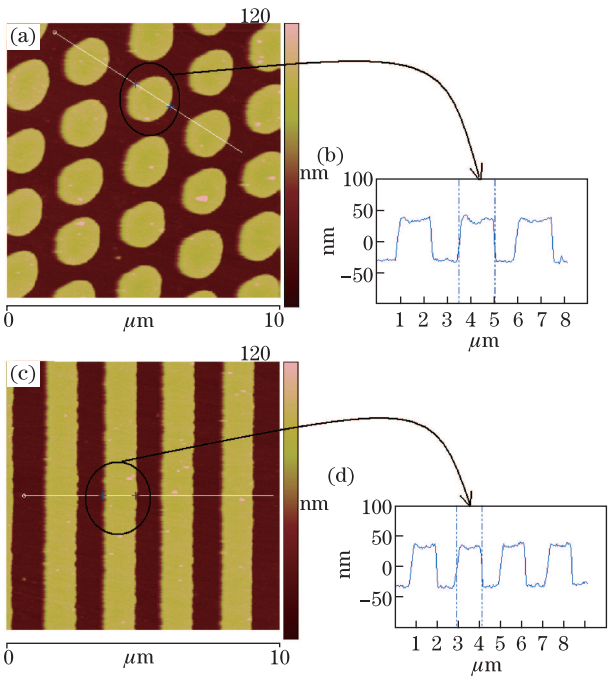

Fig. 2. AFM photos of crystalline areas after etching in 10% NaOH solution for 3 min. (a) AFM 2D photos of the etching spot in 10% NaOH solution; (b) contour lines of the etching spot marked by circle in (a); (c) AFM 2D photos of the etching line in 10% NaOH solution; (d) contour lines of the etching line marked by circle in (c).

According to the different etching rates of crystalline and amorphous states in NaOH solution, spot-shaped and line-shaped pattern structures can be obtained by the etching process. Figures 2(a) and (c) show the AFM two-dimensional (2D) photos of the spot and line obtained after etching both states in NaOH solution for 3 min. The spot and line appear to be smooth and uniform. In the contour lines shown in Figs. 2(b) and (d), both the spot and line are approximately 100 nm higher than the as-deposited film after the etching process, similar to a relief structure with a steep wall and smooth top. The crystalline state was also verified after being irradiated by laser irradiation. These structures are applicable to many fields such as optical disk mastering and grating pattern structures.

The microbump emerges when the laser power increases beyond a particular microbump threshold. Figure 3 shows the gradual change process of the microbump. Figures 3(a) and (c) are spot-shaped and line-shaped microbumps, which are induced by pulse laser and continuous laser beam, respectively. Compared with the steep wall and smooth top of the structures in Fig. 2, the structure in Fig. 3(a) appears as a regular and uniform taper-shaped structure. It begins from the rounded and smooth central dome growing out because of the laser power of 1.5 mW applied to the dome, gradually increasing the power to its maximum value of 80 nm with a laser power of 4.5 mW and laser pulse width of 50 ns. Figure 3(c) shows the line-shaped microbumps and the well-defined boundary of the area with and without laser irradiation. Figures 3(b) and (d) are the lateral photos of Figs. 3(a) and (c), respectively. Figure 3(b) shows the gradual increase in the height of the microbumps as the laser power increases. The line-shaped microbumps in Fig. 3(d) are induced by continuous laser beam with a laser power of 4.8 mW and a height of approximate 100 nm. These uniform and regular microbumps could also be used as pattern structures without undergoing etching and developing. The mechanism of the microbump is explained by the different thermal expansion coefficients between the solid state and molten state[8]. The volume thermal expansion coefficients of AIST thin film in the crystalline and molten states are estimated to be $\beta_c = 25\times10^{-6}/°C$ and $\beta_m = 25 \times 10^3/°C$, respectively. The corresponding volume thermal expansion coefficient in the molten state is approximately 10^3 times of the expansion coefficient in the solid state. Thus, when the material is melted by laser irradiation, the volume expansion caused by melting becomes obvious, which in turn finally forms the taper-shaped microbumps due to Gaussian intensity distribution of the laser beam.

Following the increase of laser power beyond another threshold, the microbump begins to form a depression or dimple in the middle. Subsequently, a rupture occurs, resulting in the formation of a deep hole due to the ablation effect when the laser power is high enough. The whole process is shown in Fig. 4(a), including the five kinds of morphology which emerge as the pulse energy increases. Figure 4(b) presents the chosen area and the corresponding contour line of the pattern units. As the laser power increases to 5.0 mW, the height of the microbumps increases to the maximum. The result is shown as the area marked as "A". When the laser energy reaches up to 5.2 mW, the depression or dimple in the middle of the microbumps emerges. This is the area marked as "B",

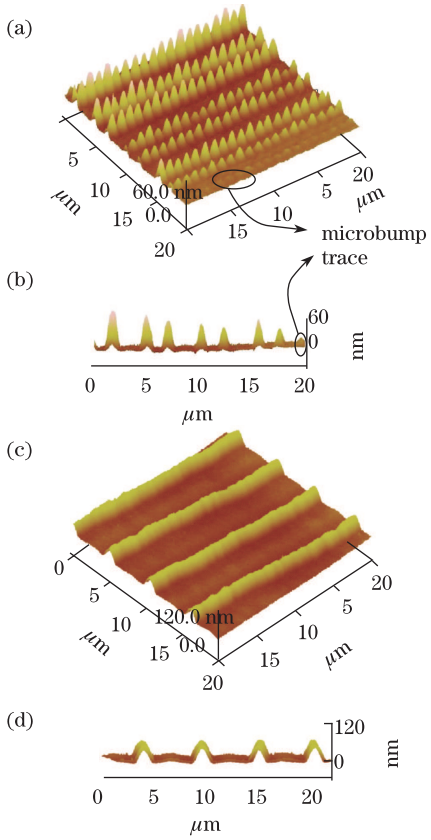

Fig. 3. Microbumps induced on AIST films by red laser (pulse laser, $\lambda = 635$ nm, NA=0.9) under different laser parameters. (a) AFM 3D photos of taper-shaped microbumps induced by different laser powers; (b) lateral photos of the microbumps in (a); (c) AFM 3D photos of line-shaped microbumps induced by continuous laser; (d) lateral photos of the line-shaped microbumps in (c).

which is a sign of the microbump rupture called rupture threshold. If the laser energy increases to 5.3 mW, the central depression gradually broadens to form a big hole in the center, similar to the area marked as "C". The hole grows larger and deeper following the increase of laser energy to 5.5 mW. Consequently, a deep-bowl shape surrounded by a high rim is formed. This is shown as the area marked as "D". All the different shape morphologies mentioned above are higher than the film surface. By adjusting the experimental parameters, we obtained uniform and regular deep-bowl shape pattern structures using laser power of 5.4 mW and pulse width of 45 ns as shown in Fig. 4(c). The diameter of the pattern unit is approximately 1 μm. Figure 4(d) shows the ring-shaped rim of the pattern structure which is approximately 50 nm higher than the surface. The hole in the center is approximately 80 nm in depth, which is very close to the thickness of the film. When the laser energy increases to a higher level of power, the ablation begins and forms the large hole as shown as the area marked "E" in Fig. 4(a). The ablated hole is approximately 80 nm below the film surface. According to previous work[8], the melting and vaporization temperatures of AIST material are only 780 and 1010 K, respectively. These are known as the melting and vaporization thresholds, which are easily ablated. In reality, ablation begins with the occurrence of depression, which at this stage mainly involves

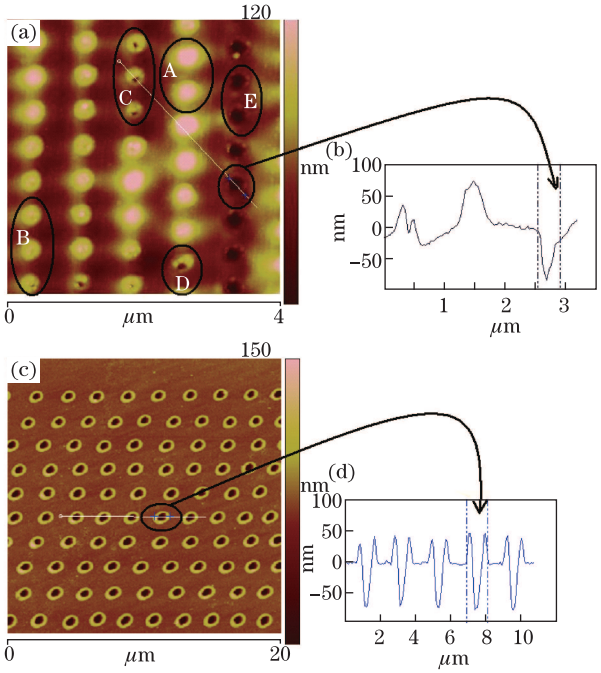

Fig. 4. Different morphologies following an increase in laser energy to certain values. (a) AFM 2D photos of the five special areas marked as "A", "B", "C", "D", and "E" corresponding to the five morphologies; (b) contour line of the area marked by a circle in (a); (c) AFM 2D photos of the deep-bowl shaped pattern structures fabricated on AIST film by red laser (pulse laser, $\lambda = 635$ nm); (d) contour lines of the chosen area marked by circle in (c).

fusion motion because of the slight ablation. Large-scale ablation would result in a big hole on the film, similar to the area marked as "D" in Fig. 4(a). It should be noted that the fabrication of various pattern structures on this material is characterized with reproducibility and efficiency. Based on this, we are certain that the result of our application will eventually find its scientific and industrial application.

In conclusion, we obtain different pattern structures on AIST phase change film as induced by laser beam. The different pattern structures are observed and analyzed by AFM. The AFM photos clearly show the gradually changing process of the pattern structures on AIST material as a function of laser energy. The photos also show several interesting threshold effects under a certain level of laser energy, such as the crystallization threshold, microbump threshold, melting threshold, rupture threshold, ablation threshold, and the different threshold effects corresponding to the different pattern structures.

This work was partially supported by the National Natural Science Foundation of China (Nos. 50772120, 60977004, and 11054001), the Shanghai Rising Star Tracking Program (No. 10QH1402700), and the Basic Research Program of China (No. 2007CB935400). The authors are also grateful to Changmeng Deng and Hao Li for their help in the etching experiment.

References

1. J. P. Moening, S. S. Thanawala, and D. G. Georgiev, Appl. Phys. A **95,** 635 (2009).

2. C. Cai, J. Huang, Y. Zhai, W. Ma, and W. Liu, Chin. Opt. Lett. **8,** (suppl.) 210 (2010).
3. J. Liu, Z. Guo, W. Liu, and H. Liu, Chin. Opt. Lett. **8,** (suppl.) 216 (2010).
4. D. Bäuerle, *Laser Processing and Chemistry* (3rd edn) (Springer, Berlin, 2000).
5. F. X. Zhai, Y. Wang, Y. Q. Wu, and F. X. Gan, Proc. SPIE **7125,** 71251W-1 (2009).
6. W. H. Wang, L. C. Chung, and C. T. Kuo, Surf. Coat. Technol. **177-178,** 795 (2004).
7. S. R. Ovshinky, Phys. Rev. Lett. **21,** 1450 (1968).
8. J. S. Wei, X. B. Jiao, F. X. Gan, and M. F. Xiao, J. Appl. Phys. **103,** 124516 (2008).
9. N. Wuttig and C. Steimer, Appl. Phys. A **87,** 411 (2007).
10. X. B. Jiao, J. S. Wei, F. X. Gan, and M. F. Xiao, Appl. Phys. A **94,** 627 (2009).
11. W. Welnic, S. Botti, L. Reining, and M. Wuttig, Phys. Rev. Lett. **98,** 236403 (2007).
12. V. G. Karpov, Y. A. Kryukov, S. D. Savransky, and I. V. Karpov, Appl. Phys. Lett. **90,** 123504 (2007).
13. H. Huang, F. Y. Zuo, F. X. Zhai, Y. Wang, T. S Lai, Y. Q. Wu, and F. X. Gan, J. Appl. Phys. **106,** 063501 (2009).
14. V. Weidenhof, I. Friedrich, S. Ziegler, and M. Wuttig, J. Appl. Phys. **86,** 5879 (1999).
15. W. K. Njoroge, H. W. Woltgens, and M. Wuttig, J. Vac. Sci. Technol. A **20,** 230 (2002).
16. S. Raoux, R. M. Shelby, J. J. Sweet, B. Munoz, M. Salinga, Y. C. Chen, Y. H. Shih, E. K. Lai, and M. H. Lee, Microelectron. Eng. **85,** 2330 (2008).
17. J. S. Wei and F. X. Gan, Thin Solid Films **441,** 292 (2003).